

Influence of Ethanol on Lipid/Sterol Membranes: Phase Diagram Construction from AFM Imaging

Juan M. Vanegas,[†] Roland Faller,^{†,‡} and Marjorie L. Longo^{*,†,‡}

[†]*Biophysics Graduate Group, College of Biological Sciences and* [‡]*Department of Chemical Engineering and Materials Science, University of California, Davis, California 95616*

Received March 29, 2010. Revised Manuscript Received May 25, 2010

Herein we develop a sample preparation approach that enables the use of supported lipid bilayers for the quantitative study of the influence of ethanol (0–20 vol %) on the phase behavior of phospholipid (DPPC)/sterol (ergosterol, 0–20 mol %) bilayers. Three coexisting phases were observed with tapping-mode atomic force microscopy: gel (L_{β}'), liquid-ordered (L_o), and interdigitated (L_{β}'/I). High-resolution imaging permitted the construction of a refined phase diagram for DPPC/ergosterol/ethanol and the observation of L_o – L_{β}' phase separation that has not been observed using optical techniques. Our results quantitatively show the concentration regime where ergosterol protects the membrane by reducing the membrane fraction that is interdigitated in the presence of ethanol.

Introduction

Fermenting microorganisms, including yeasts, contain 10–25 mol % ergosterol (the predominant sterol) in their plasma membranes and are usually exposed to as much as 15 vol % ethanol during fermentation. Ergosterol levels in yeast membranes are known to increase as a survival response to ethanol exposure.¹ Sterols such as ergosterol or cholesterol, which form a liquid-ordered phase with lipids, may modulate ethanol–membrane interactions, protecting membranes from the deleterious effects of alcohols.^{1–4} In particular, an interdigitated phase of reduced thickness^{5–7} can form in lipid bilayer membranes in the presence of short-chain alcohols and other volatile anesthetics. At lower anesthetic concentrations, relevant to mammals, the anesthetic effects of these molecules may be caused by directly targeting membrane proteins such as ligand-gated ion channels^{8,9} or by indirect interaction with these proteins through physical changes in the lipid membrane.¹⁰

Alcohol- and other anesthetic-induced interdigitation has been studied in unilamellar,^{11,12} multilamellar,^{5,7,11,13} and supported lipid bilayers.^{14–16} Molecular dynamics simulations of lipid bilayers with alcohols have also provided some insight into the molecular interactions and the structure of the interdigitated

phase.^{2,17,18} Inducing interdigitation in supported gel-phase lipid bilayers requires ethanol concentrations that are 5–10 times higher than for “free bilayers” with long incubation periods¹⁵ or heating to above the main phase-transition temperature (T_m) after the addition of ethanol.¹⁴ Furthermore, even with these treatments, the extent of interdigitation is lower compared to that for unsupported unilamellar and multilamellar systems. Previous AFM studies of the anesthetic-induced interdigitation of supported DPPC (1,2-dipalmitoyl-*sn*-glycero-3-phosphocholine) bilayers have provided details of bilayer thickness and material properties such as viscoelasticity.¹⁶ However, because of this concentration discrepancy, AFM of supported lipid bilayers has not significantly added to our knowledge of the phase behavior of membrane–alcohol systems. In addition, no previous AFM studies have examined lipid–sterol membranes in the presence of ethanol to the best of our knowledge.

In the present work, we develop a sample preparation methodology to minimize the influence of the support and eliminate the ethanol concentration discrepancy for the induction of interdigitation in supported DPPC lipid bilayers. Subsequently, we investigate with AFM the ethanol-induced interdigitation of pure DPPC and DPPC/ergosterol supported bilayers, providing for the first time high-resolution imaging (on the nanometer scale) of the coexistence of the gel (L_{β}'), liquid-ordered (L_o), and interdigitated (L_{β}'/I) phases. With these highly detailed images, we calculate the area fractions of the different phases in order to refine the DPPC/ergosterol/ethanol phase diagram and better define the concentration region over which ergosterol protects the membrane from the interdigitation caused by ethanol.

Materials and Methods

Details of the sample preparation and experimental measurements are provided in the Supporting Information.

Results and Discussion

Influence of the Support on DPPC and DPPC/Ethanol Phase Behavior. Supported DPPC bilayers, prepared by vesicle fusion in nanopure water at 65 °C and imaged at 23 °C using tapping-mode AFM (TM AFM), displayed the expected L_{β}' phase of DPPC interspersed with a phase of lower height (approximately 1.4 nm lower) as shown in Figure 1A. The thickness difference between L_{β}' and a pressure-induced L_{β}'/I phase has

*To whom correspondence should be addressed. E-mail: mllongo@ucdavis.edu. Telephone: (530) 754-6348. Fax: (530) 752-1031.

- (1) Bisson, L. *Am J. Enol. Viticult.* **1999**, *50*, 107–119.
- (2) Dickey, A. N.; Yim, W. S.; Faller, R. J. *Phys. Chem. B* **2009**, *113*, 2388–2397.
- (3) Rosser, M.; Lu, H. M.; Dea, P. *Biophys. Chem.* **1999**, *81*, 33–44.
- (4) Komatsu, H.; Rowe, E. S. *Biochemistry* **1991**, *30*, 2463–2470.
- (5) Simon, S.; McIntosh, T. *Biochim. Biophys. Acta* **1984**, *773*, 169–172.
- (6) Slater, J. L.; Huang, C. H. *Prog. Lipid Res.* **1988**, *27*, 325–359.
- (7) Adachi, T.; Takahashi, H.; Ohki, K.; Hatta, I. *Biophys. J.* **1995**, *68*, 1850–1855.
- (8) Eckenhoff, R. G.; Johansson, J. S. *Pharmacol. Rev.* **1997**, *49*, 343–367.
- (9) Sirois, J. E.; Lei, Q.; Talley, E. M.; Lynch, C. 3.; Bayliss, D. A. *J. Neurosci.* **2000**, *20*, 6347–6354.
- (10) Cantor, R. S. *Biophys. J.* **2001**, *80*, 2284–2297.
- (11) Vierl, U.; Löbbecke, L.; Nagel, N.; Cevc, G. *Biophys. J.* **1994**, *67*, 1067–1079.
- (12) Tierney, K. J.; Block, D. E.; Longo, M. L. *Biophys. J.* **2005**, *89*, 2481–2493.
- (13) Nambi, P.; Rowe, E. S.; McIntosh, T. *Biochemistry* **1988**, *27*, 9175–9182.
- (14) Mou, J.; Yang, J.; Huang, C.; Shao, Z. *Biochemistry* **1994**, *33*, 9981–9985.
- (15) Leonenko, Z. V.; Cramb, D. T. *Can. J. Chem.* **2004**, *82*, 1128–1138.
- (16) Leonenko, Z.; Finot, E.; Cramb, D. T. *Biochim. Biophys. Acta* **2006**, *1758*, 487–492.
- (17) Dickey, A. N.; Faller, R. J. *Polym. Sci., Polym. Phys.* **2005**, *43*, 1025–1032.
- (18) Kranenburg, M.; Vlaar, M.; Smit, B. *Biophys. J.* **2004**, *87*, 15961605.

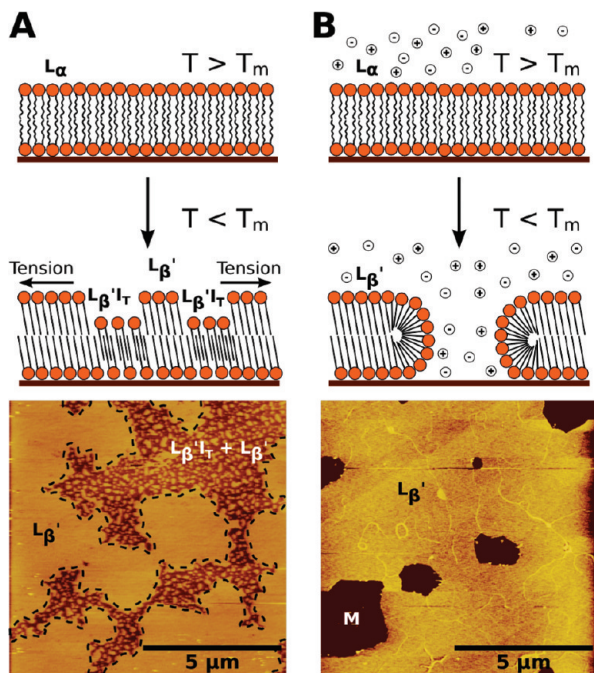


Figure 1. Tapping-mode AFM images of supported DPPC bilayers on mica deposited at 65 °C and imaged at 23 °C. (A) Bilayer prepared in nanopure water where a tension-induced interdigitated ($L_{\beta}'I_T$) phase is interspersed with the L_{β}' phase because of the interaction with the support and lateral tension. (B) Bilayer prepared in a PBS solution where a uniform phase is observed to coexist with defects exposing the mica (M) support.

been reported to be 1.4–1.5 nm,^{19,20} in good agreement with our measurement. As illustrated in Figure 1A, the presence of this lateral tension-induced (which acts as pressure normal to the bilayer) interdigitated ($L_{\beta}'I_T$) phase may be the result of a combination of two factors: the interaction with the support²¹ and the tension created by having to cover a larger surface area as the bilayer condensed from the higher area per lipid L_{α} (liquid disordered) phase to the lower area per lipid L_{β}' phase during cooling. Exchanging water with a 15 vol % ethanol–water solution yielded no noticeable change as shown in Figure S1, in disagreement with the complete transition to the $L_{\beta}'I$ phase for this ethanol concentration documented for unilamellar GUVs¹² and multilamellar dispersions.¹¹

However, if micrometer-scale defects were present (Figure 2A), achieved by adding a heating–cooling cycle to eject material, the exchange of water for an ethanol solution introduced a new phase of lower height (approximately 1.6 nm lower than the L_{β}' phase) with area fractions of approximately 0.3 (15 vol % ethanol) and 0.4 (30 vol % ethanol) as shown in Figure 2B,C respectively. This new phase is the ethanol-induced interdigitated ($L_{\beta}'I$) phase, based upon the height difference with the L_{β}' phase.¹⁴ Unfortunately, these area fractions are in disagreement with the known phase behavior of unsupported lipid bilayers (the $L_{\beta}'I$ phase should be the only phase present^{11,12}), and the continued presence of tension-induced $L_{\beta}'I_T$ interferes with measurements of the interdigitated area because the $L_{\beta}'I$ and $L_{\beta}'I_T$ phases are very similar in height and cannot be easily discerned.

Influence of Ethanol on the DPPC Phase Behavior: Reducing the Influence of the Support. When prepared by vesicle

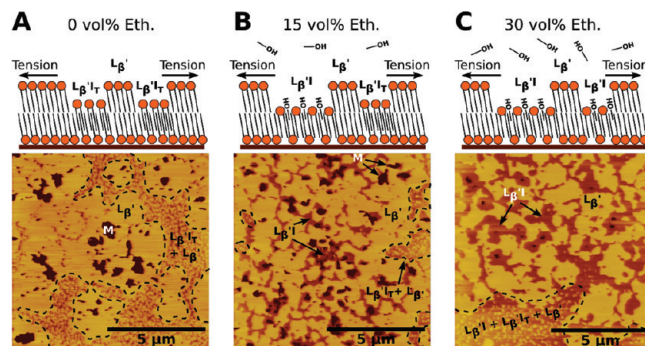


Figure 2. (A) Pure DPPC bilayer deposited in nanopure water at 65 °C, cooled to 23 °C, reheated to 50 °C, and cooled again to 23 °C, thereby exposing mica (M). (B) After exchange of the water with a 15 vol % ethanol solution, the ethanol-induced interdigitated ($L_{\beta}'I$) phase was introduced. (C) After exchange with a 30 vol % ethanol solution.

fusion in a 65 °C phosphate-buffered saline (PBS) solution (pH 7.4), supported DPPC bilayers imaged at 23 °C were of a uniform thickness and coexisted with a large number of defects (Figure 1B). As illustrated in Figure 1B, the presence of salt in the solution condenses the bilayer,²² which may help to overcome the lateral tension in the bilayer and induce the formation of defects, exposing mica, instead of forming the $L_{\beta}'I_T$ phase. The average thickness of L_{β}' DPPC bilayers in PBS solution was 5.3 ± 0.3 nm, consistent with the 4.8 nm²³ bilayer thickness (from diffraction data) and a water layer of 0.5 nm²⁴ between the bilayer and the mica support. Table S1 lists statistically measured heights of lipid phases. Rarely, ripples were observed (Figure S2A) with an approximate wavelength of 15 nm, consistent with the characteristics of the ripple phase (P_{β}') as previously reported.^{25,26} When ethanol was included in the PBS solution, supported DPPC bilayers displayed ethanol-dependent phase behavior consistent with unsupported bilayers.^{11,12} Specifically, as demonstrated in Figure S2, we observed a small area fraction (0.10 ± 0.08) of the $L_{\beta}'I$ phase in 5 vol % ethanol, and in 15 vol % ethanol, the majority of the area was interdigitated $L_{\beta}'I$ (area fraction 0.93 ± 0.09). Table 1 lists the statistically measured area fractions of lipid phases. We speculate that the ethanol partitioned around the lipid headgroups before the vesicles adhered to the support and the salt effectively reduced the bilayer–support interaction, thereby resembling the free lipid bilayer environment. We also speculate that defects had little impact on the phase behavior because they were generally large (greater than 1 to 2 μm) and thus the edge to membrane area ratio was small. Therefore, in the phase diagram construction, all samples were prepared by vesicle fusion in ethanol/PBS buffer solutions at 65 °C, followed by cooling to 23 °C.

Influence of Ethanol on DPPC/Ergosterol Phase Behavior: Phase Diagram Construction. Three phases exist in DPPC/ergosterol bilayers in ethanol solutions at 23 °C: L_{β}' (gel), $L_{\beta}'I$ (interdigitated), and L_o (liquid-ordered) based upon DPPC/ergosterol²⁷ and DPPC/ethanol¹¹ phase diagrams. Although the previously reported DPPC/ergosterol/ethanol phase diagram

(22) Böckmann, R. A.; Hac, A.; Heimburg, T.; Grubmüller, H. *Biophys. J.* **2003**, *85*, 1647–1655.

(23) Nagle, J. F.; Tristram-nagle, S. *Biochim. Biophys. Acta* **2000**, *1469*, 159–195.

(24) Watkins, E.; Miller, C.; Mulder, D.; Kuhl, T.; Majewski, J. *Phys. Rev. Lett.* **2009**, *102*, 1–4.

(25) Sun, W.; Tristram-Nagle, S.; Suter, R.; Nagle, J. *Proc. Natl. Acad. Sci. U.S.A.* **1996**, *93*, 7008–7012.

(26) Kaasgaard, T.; Leidy, C.; Crowe, J. H.; Mouritsen, O. G.; Jørgensen, K. *Biophys. J.* **2003**, *85*, 350–360.

(27) Hsueh, Y.; Gilbert, K.; Trandum, C.; Zuckermann, M.; Thewalt, J. *Biophys. J.* **2005**, *88*, 1799–1808.

(19) Seto, H.; Hishida, M.; Nobutou, H.; Yamada, N. L.; Nagao, M.; Takeda, T. *J. Phys. Soc. Jpn.* **2007**, *76*, 054602.

(20) Braganza, L. F.; Worcester, D. L. *Biochemistry* **1986**, *25*, 2591–6.

(21) Xing, C.; Ollila, O. H.; Vattulainen, I.; Faller, R. *Soft Matter* **2009**, *5*, 3258–3261.

Table 1. Area Fractions (f)

composition (mol %)	ethanol (vol %)	fL_o	fL_{β}'	$fL_{\beta}'I$
100% DPPC–0% ergo				
Figure S2	0		uniform phase	
Figure S2	5		0.90 ± 0.08	0.10 ± 0.08
Figure 3A	10		0.21 ± 0.13	0.79 ± 0.13
Figure S2	15		0.07 ± 0.09	0.93 ± 0.09
90% DPPC–10% ergo				
Figure 3E	0		spinodal decomposition region ^a	
Figure 3D	5	0.45 ± 0.03	0.55 ± 0.03	0.00 ± 0.00
Figure 3C	10	0.39 ± 0.05	0.52 ± 0.05	0.09 ± 0.05
Figure 3B	12.5	0.16 ± 0.03		0.84 ± 0.03
80% DPPC–20% ergo				
Figure S4	0		uniform phase	
Figure S4	5		uniform phase	
Figure 3H	10		uniform phase	
Figure 3G	15	0.84 ± 0.18	0.11 ± 0.11	0.05 ± 0.07
Figure 3F	20	0.84 ± 0.09		0.16 ± 0.09

^a Area fractions for this concentration could not be accurately calculated, yet L_{β}' appears to have a larger area fraction than the L_o phase

(Figure S5¹²) was based upon the mechanical behavior (area compressibility modulus) and visual appearance of GUVs, the present work is based upon topographical data on the nanometer scale provided by AFM imaging. See Figures S2–S4 for a full set of images and sample height cross-sections. The phase separation between L_{β}' and $L_{\beta}'I$ (Figure 3A) or L_o and $L_{\beta}'I$ (Figures 3B and 3F) could be easily distinguished because the height differences (Figure S6 and Table S1) were consistently 1.9 ± 0.2 nm, in good agreement with previously reported AFM values of 1.9–2.0 nm^{14,15} ($L_{\beta}'-L_{\beta}'I$ height difference). $L_{\beta}'-L_o$ phase separation within the same sample could be distinguished by the greater height of the L_{β}' phase, although the contrast was limited by the small height difference between the two lipid phases (close to 0.1 nm). The tapping phase (an angular phase shift in the tip oscillation and measurement of sample properties such as viscoelasticity) played an important role in distinguishing these two lipid phases because the L_{β}' and L_o phases consistently produced positive and negative phase shifts, respectively, and often produced higher-contrast images in comparison to the height images. All TM AFM images presented here correspond to heights except for Figures 3G and S4D, where the height and tapping-phase data were combined to produce a higher-contrast image (Figure S7).

Using the area fractions of each phase (Table 1), we constructed a refined phase diagram for DPPC/ergosterol/ethanol (Figure 3) on the basis of the phase diagram reported by Tierney et al.¹² and the ethanol-free DPPC/ergosterol phase diagram by Hsueh et al.²⁷ As demonstrated in Figure 3C,G, three distinct regions/phases coexisted in supported DPPC bilayers containing 10 and 20 mol % ergosterol in 10 and 15 vol % ethanol solutions, respectively. This observation is in good agreement with the presence of $L_o + L_{\beta}' + L_{\beta}'I$ coexistence in the phase diagram (Figure S5) by Tierney et al.¹² for free bilayers. The measured area fraction of each phase under these conditions (Table 1) allowed us to define the right boundary and upper and lower vertices of a three-phase triangle. To use area fractions to define phase boundaries, we assumed that the L_o and L_{β}' phases have the same area per DPPC molecule (because the two phases are almost indistinguishable in height) and that the area per DPPC molecule in the $L_{\beta}'I$ phase is 1.5 times larger than that in the L_{β}' phase. (See the Supporting Information for the calculation.)

Two regions of height corresponding to the $L_{\beta}'I$ and L_o phases coexisted, as demonstrated in Figure 3B,F, in supported DPPC bilayers containing 10 and 20 mol % ergosterol in 12.5 and 20 vol % ethanol solutions, respectively. This observation is in

good agreement with the presence of $L_o + L_{\beta}'I$ coexistence in the phase diagram (Figure S5) by Tierney et al.¹² for free bilayers. Respectively, the measured area fractions (Table 1) for these two conditions were used to define the lower left vertex of the three-phase triangle and lower/upper boundaries of the $L_o + L_{\beta}'I$ coexistence region assuming that the tie line under that condition lies parallel to the left boundary of the three-phase triangle. The large height difference (2.0 nm) between the $L_{\beta}'I$ and L_o phases at 20 mol % ergosterol in 20 vol % ethanol indicates that there may not be a critical point close to this area; therefore, the left side of the $L_o + L_{\beta}'I$ region is left open.

The upper right boundary of the $L_o + L_{\beta}'$ to L_o transition was defined by the observation of a single uniform phase for 20 mol % ergosterol bilayers in 0, 5, and 10 vol % ethanol solutions, as demonstrated in Figure 3H, and by using the L_{β}' and L_o area fractions (Table 1) for 10 mol % ergosterol bilayers in 5 vol % ethanol solutions (Figure 3D). A 2–4-fold increase in the area compressibility modulus along this proposed boundary can be observed in the phase diagram by Tierney et al.¹² (Figure S5).

Gel–Liquid Ordered-Phase Coexistence and DPPC–Ergosterol Complex. Our phase diagram (Figure 3) indicates that the $L_o + L_{\beta}'$ to L_o transition, in the absence of ethanol, takes place at approximately 17 mol % ergosterol. However, linear extrapolation of the DPPC/ergosterol²⁷ phase diagram (obtained from multilamellar dispersions) to 23 °C suggests that this transition takes place at around 30 mol % ergosterol. Each of these ergosterol mole fractions corresponds approximately to the site-percolation threshold of an ergosterol–phospholipid complex with a particular stoichiometry. Complexes^{29,30} have been proposed with lipid to sterol stoichiometries of 1:1 or 2:1.³¹ At 16.7 and 25 mol % ergosterol, 50% of the hexagonal lattice sites would be occupied by complexes for the 2:1 (see Figure S8 for a schematic representation) and 1:1 stoichiometries, respectively. Occupation of 50% is the site percolation threshold for a 2D hexagonal (triangular) lattice with a random occupation of sites,³² indicating that the L_o phase is characterized by the continuity of sterol–phospholipid complexes. Alternatively, each ergosterol mole fraction corresponds approximately to the stoichiometry

(28) Marsh, D. *Biochim. Biophys. Acta* **2009**, *1788*, 2114–2123.

(29) Hung, W.; Lee, M.; Chen, F.; Huang, H. W. *Biophys. J.* **2007**, *92*, 3960–3967.

(30) Radhakrishnan, A.; McConnell, H. *Proc. Natl. Acad. Sci. U.S.A.* **2005**, *102*, 12662–12666.

(31) Pan, J.; Nagle, J. F.; Mills, T. T.; Tristram-Nagle, S. *Phys. Rev. Lett.* **2008**, *100*, 1–4.

(32) Sykes, M. F.; Essam, J. W. *J. Math. Phys.* **1964**, *5*, 1117–1127.

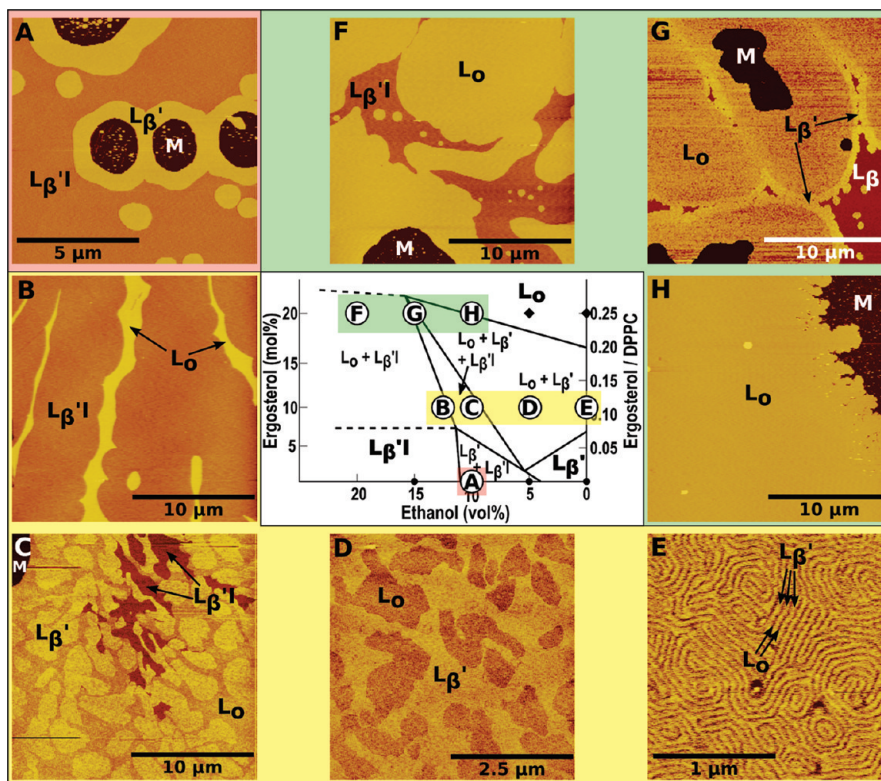


Figure 3. Proposed DPPC/ergosterol/ethanol phase diagram determined using area fractions (Table 1) and presented in the convention of Marsh.²⁸ (A–H) Selected tapping-mode AFM images showing domains and phase separation of the phases of interest (L_{β}' , $L_{\beta}'I$, and L_o). AFM images for solid dot and diamond data points are shown in Figures S2 and S4, respectively. All supported lipid bilayers were prepared by vesicle fusion in ethanol/PBS buffer solutions at 65 °C and cooled to 23 °C. Areas labeled with M show defects where the mica support is exposed.

of a nonrandomly distributed superlattice (SL). At a certain critical concentrations (C_r), which can be calculated from the geometrical organization of the SL, the membrane properties undergo sharp changes as the lipids organize into an SL.^{33,34} Calculated C_r values close to our observed transition occur at 15.4 and 20.2 mol %³³ and at 25 and 33 mol % in comparison to the 30 mol % transition.

The location of a transition from L_o domains to L_{β}' domains takes place at roughly 10 mol % ergosterol where we observed bands (~ 50 nm wavelength and ~ 0.5 nm amplitude) that oscillate between the L_{β}' and L_o phases (Figure 3E). The morphology suggests formation by spinodal decomposition. The L_{β}' phase appears to have a larger area fraction than the L_o phase, consistent with our phase diagram. This type of morphology has been observed in highly oriented samples through X-ray diffraction³⁵ and cryo-electron microscopy³⁶ in DPPC/cholesterol bilayers. This phase separation indicates that the spinodal region is roughly centered between the bimodal L_{β}' to $L_{\beta}' + L_o$ and $L_{\beta}' + L_o$ to transitions of approximately 8 mol %²⁷ and 17 mol % ergosterol, respectively. The small length scale of phase separation in this spinodal region and the lack of domain coarsening indicate that the free-energy difference driving demixing is small and the transition is only weakly first order, which explains the absence of fluorescence microscopy observation of L_{β}' and L_o coexistence in binary lipid–sterol mixtures.

Conclusions

Our results show good agreement with previous findings obtained from unsupported lipid bilayers of DPPC/ethanol¹¹ (multilamellar dispersions) and DPPC/ergosterol/ethanol¹² (GUVs), and with high-resolution images obtained from TM AFM, we can describe in detail the various phases observed and define the phase-transition boundaries. Our method of preparation played an important role in obtaining agreement with unsupported studies and should be taken into account in future investigations of the effects of perturbing molecules on supported bilayers. The protective effect of ergosterol against the harmful effects of ethanol is clearly observed because higher ethanol concentrations are needed to induce interdigitation as ergosterol levels increase. Our results may also help us to understand the phase diagrams of ternary lipid mixtures, and future work may be headed toward investigating the interaction of ethanol with membranes of higher complexity.

Acknowledgment. This work was supported by USDA grant 2007-02140. We thank Dr. David Block for helpful discussions.

Supporting Information Available: Materials and methods used for the preparation of the supported lipid bilayers and other experimental details as well as supplemental figures including a full set of images, the previous DPPC/ergosterol/ethanol phase diagram from Tierney et al.,¹² the height distribution from an image, height and tapping-phase images from one sample, a schematic representation of the DPPC/ergosterol complex, and a table with measured thicknesses of the different phases. This material is available free of charge via the Internet at <http://pubs.acs.org>.

(33) Chong, P. L. *Proc. Natl. Acad. Sci. U.S.A.* **1994**, *91*, 10069–10073.

(34) Chong, P. L.; Zhu, W.; Venegas, B. *Biochim. Biophys. Acta* **2009**, *1788*, 2–11.

(35) Karmakar, S.; Raghunathan, V. *Phys. Rev. Lett.* **2003**, *91*, 18–21.

(36) Lentz, B. R.; Barrow, D. A.; Hoehli, M. *Biochemistry* **1980**, *19*, 1943–1954.